

On homogenization of electromagnetic crystals formed by uniaxial resonant scatterers

Pavel A. Belov

*Mobile Communication Division, Telecommunication Network Business, Samsung Electronics Co., Ltd.,
94-1, Imsoo-Dong, Gumi-City, Gyeong-Buk, 730-350, Korea*

Constantin R. Simovski

*Photonics and Optoinformatics Department, St. Petersburg State University of Information Technologies,
Mechanics and Optics, Sablinskaya 14, 197101, St. Petersburg, Russia*

(Dated: November 20, 2018)

Dispersion properties of electromagnetic crystals formed by small uniaxial resonant scatterers (magnetic or electric) are studied using the local field approach. The goal of the study is to determine the conditions under which the homogenization of such crystals can be made. Therefore the consideration is limited by the frequency region where the wavelength in the host medium is larger than the lattice periods. It is demonstrated that together with known restriction for the homogenization related with the large values of the material parameters there is an additional restriction related with their small absolute values. From the other hand, the homogenization becomes allowed in both cases of large and small material parameters for special directions of propagation. Two unusual effects inherent to the crystals under consideration are revealed: flat isofrequency contour which allows subwavelength imaging using canalization regime and birefringence of extraordinary modes which can be used for beam splitting.

PACS numbers: 78.20.Ci, 42.70.Qs, 42.25.Gy

I. INTRODUCTION AND PROBLEM FORMULATION

The problem of homogenization of bulk arrays of small scatterers operating in the applied field as dipoles (electric or magnetic) has a long history. One can recall here the classical works of Lorentz, Madelung, Ewald and Oseen. However, in what concerns the homogenization of arrays of small resonant scatterers these classical results were revised in 1970-s taking into account the possible shortening the propagating wave at the resonance and the strong mutual coupling of resonant particles. It was done in the seminal work by Sipe and Kranendonk [1]. In 1990-s the interest to this problem was renewed by extensive studies of bianisotropic composites (see e.g. in [2] and [3]). The metal bianisotropic particles (chiral particles and omega particles) have small resonant size at microwaves due to their complex shape (they include a wire ring and straight wire portions). However, the known studies of their homogenization are mainly referred to the non-regular arrays. This can be explained by specific applications of microwave bianisotropic composites (as absorbers or antiradar coverings). The works like [4] concerning the regular bianisotropic lattices do not consider effects of particles resonance. Briefly, the homogenization problem for resonant scatterers has not been studied enough. However, it is becoming very important now due to the following reasons.

The first one is the rapid development of nanotechnologies. It becomes possible to prepare the lattices of metallic nano-particles operating at the frequencies rather close to that of the plasmon resonance of the individual particle. Recently, a significant amount of works has been devoted to 1D arrays (chains) of silver or gold

particles which were found prospective for subwavelength guiding the light (see e.g. [5] and the list of references of this work). It is evident that the 2D and 3D lattices of metal nano-particles provide potentially even more broad scope of optical applications than the chains. If the homogenization of a 3D lattice is possible then one can use the basic knowledge on the continuous media and apply it to the lattices. This approach can be rather instructive and we demonstrate below its example. In the present paper we study the case of microwave scatterers, but this is only an illustration of the theory. Similar results can be obtained for the optical range, too. The electric scatterers of small resonant size are already known in optics, and the possibility to create the small resonant scatterers with magnetic properties was recently shown in work [6].

The second motivation of the present research is related with the intensive studies of the so-called left-handed media [7]. The left-handed medium (LHM) is an effective continuous medium with simultaneously negative permittivity and permeability. The all-angle negative refraction and backward waves are inherent to such media. The interest to these artificial materials was evoked by seminal work of Pendry [8] indicating the opportunity of the subwavelength imaging using a slab of LHM. The most loud realization of LHM is a uniaxial version of this medium studied in works [9],[10],[11] and others. This structure is composed from two components playing the roles of the building blocks. The first block (responsible for negative permittivity) is a wire medium [12–14] and the second block (responsible for negative permeability) is a lattice of the split-ring resonators (SRR:s) [15]. The SRR:s are small magnetic scatterers experiencing a two-time derivative Lorentz-type resonance. As a result, the permeability of the struc-

ture can take negative values within the resonance band of SRR:s. This structure operates, however, as a LHM only in the plane orthogonal to wires (and for an only polarization of the wave). The reason of that is the strong spatial dispersion inherent to wire media at all frequencies [16]. This effect makes the axial component of the wire medium permittivity depending on the propagation direction. Only for the waves propagating in the orthogonal plane this permittivity component is definitely negative until the so-called plasma frequency and the structure suggested in [9] can be treated as a LHM only in this special case.

In order to obtain a variant of LHM operating in three dimensions some attempts to use small resonant electric scatterers together with magnetic ones [17] as well as the bianisotropic scatterers [18–20] were made. The samples of LHM obtained in [18, 20] demonstrate high losses in the LHM regime and this makes the known variants of isotropic LHM not very interesting.

However, if the goal is to observe negative refraction and backward waves, and to obtain subwavelength images in three dimensions, then the isotropic LHM is not an only solution. These effects can be obtained in anisotropic structures, too. And not only at high frequencies. The so-called indefinite media (in which the principal components of permittivity and permeability tensors have different signs) were studied in works [21–23]. These media offer variety of effects including negative refraction, backward wave effect, near field focusing, high-impedance surface reflection, etc. Anisotropy of the media introduces additional freedom in manipulation by its dispersion and reflection properties [24]. Even a uniaxial media with negative permittivity along its axis allows to observe effects of negative refraction and backward wave with respect to the interface [25]. The theoretical results [21–23] do not prove that the structure composed by wire medium and SRR:s will demonstrate these effects in practice. On the contrary, from [16] and [25] it is evident that these effects (which should exist in a continuous uniaxial medium with negative axial permittivity) are absent in wire media. In the same time, a lattice of uniaxial electric scatterers oriented in parallel allows to obtain the negative axial permittivity for all directions of propagation (i.e. without spatial dispersion). If such a lattice substitutes the wire medium in the structure reported in [9, 10] then the effects predicted in [21–23] for continuous indefinite media can be obtained in practice. This is the second reason of the present study.

In the current paper dispersion properties of electromagnetic crystals formed by orthorhombic lattices of uniaxial magnetic or electric scatterers are studied. The orientation of scatterers along one of the crystal axes is considered. Geometry of the structure is presented in Fig. 1. As an example of magnetic scatterers we have chosen the SRR:s [9, 10, 15] (see Fig. 2). The electric dipoles are represented by the short inductively loaded wires (ILW) [17] (see Fig. 3).

An analytical model based on dipole approximation

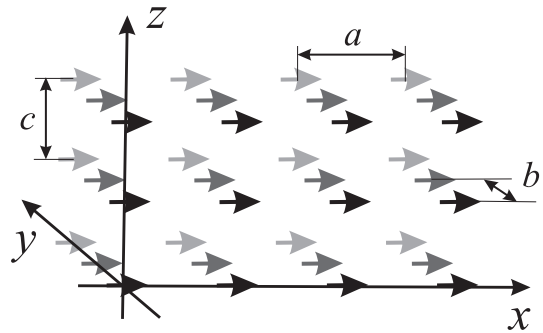


FIG. 1: Geometry of an electromagnetic crystal. The arrows show directions of dipole moments of the uniaxial scatterers.

and local field approach is introduced. The dipole approximation (magnetic dipoles describing SRR:s and electric dipoles describing ILW:s) restricts the dimensions of inclusions to be much smaller than wavelength in the host media. The local field approach allows to take into account the dipolar interactions between scatterers exactly. It makes possible accurate studies of lattice resonances. The results allows to examine when the structure corresponds to its homogenized model of local uniaxial media and when not.

It is well known that the lattices of resonant scatterers (though they do not exhibit the spatial dispersion at all frequencies unlike wire media) can experience spatial dispersion at low frequencies as compared to the spatial resonance of the lattice. This is the case when the wavelength in the medium becomes comparable with lattice period [1]. This results on resonance stop-band [1] and on appearance of complex modes within it [19, 26]. This makes the homogenization impossible within a sub-band belonging to the resonance band. In the present work we do not pay attention to the complex modes. The comparison of the original lattice and its homogenized model is made using the technique of isofrequency contours. Such an approach allows to check correspondence between properties of the structures under consideration and their homogenization models.

Uniaxial media with negative permittivity (or permeability) along its axis and positive permittivity (or permeability) in the transversal plane has the isofrequency contours of hyperbolic form [21–24]. These isofrequencies correspond to the negative refraction [22, 23]. If both original lattice and its homogenized model possess such isofrequencies then they both possess the negative refraction. More generally, if the homogenized model of the lattice keeps (at least approximately) the same isofrequency contours, then the homogenization is allowed. If the homogenization dramatically change them the homogenization is forbidden. This is the main idea of our approach.

II. MODELS OF INDIVIDUAL SCATTERERS

The geometries of the SRRs and ILW are presented in Fig. 2 and Fig. 3, respectively. Since the dipoles moments of all scatterers are directed along x (see Fig. 1) an individual scatterer can be characterized by scalar polarizability α relating the dipole moment with the local field (external field applied to a scatterer).

A. Split-Ring Resonators

The SRR considered in [9, 10, 15] is a pair of two coplanar broken rings (see Fig.2). Since the two loops are not

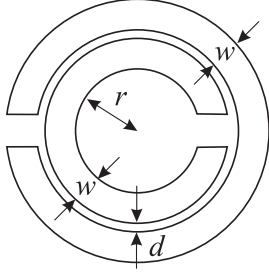


FIG. 2: Geometry of a Split-Ring-Resonator

identical the analytical models for such SRR:s are rather cumbersome [27, 28]. In fact, such SRR can not be described as a purely magnetic scatterer, because it exhibits bianisotropic properties and has resonant electric polarizability [27, 28] (see also discussion in [29]). However, the electric polarizability and bianisotropy of SRR is out of the scope of this paper. We neglect these effects and consider an ordinary SRR as a magnetic scatterer. The analytical expressions for the magnetic polarizability $\alpha(\omega)$ of SRRs with geometry plotted in Fig.2 were derived and validated in [28]. The final result reads as follows:

$$\alpha(\omega) = \frac{A\omega^2}{\omega_0^2 - \omega^2 + j\omega\Gamma}, \quad A = \frac{\mu_0^2 \pi^2 r^4}{L + M}, \quad (1)$$

where ω_0 is the resonant frequency of magnetic polarizability:

$$\omega_0^2 = \frac{1}{(L + M)C_r},$$

L is inductance of the ring (we assume that both rings have the same inductance):

$$L = \mu_0 r \left[\log \left(\frac{32R}{w} \right) - 2 \right],$$

M is mutual inductance of the two rings:

$$M = \mu_0 r \left[(1 - \xi) \log \left(\frac{4}{\xi} \right) - 2 + \xi \right], \quad \xi = \frac{w + d}{2r},$$

C_r is the effective capacitance of the SRR:

$$C_r = \varepsilon_0 \frac{r}{\pi} \operatorname{arccosh} \left(\frac{2w}{d} \right),$$

Γ is the radiation reaction factor:

$$\Gamma = \frac{A\omega k^3}{6\pi\mu_0},$$

r is the inner radius of the inner ring, w is the width of the rings, d is distance between the edges of the rings (see Fig.2), ε_0 and μ_0 are permittivity and permeability of the host media, and $k = \omega\sqrt{\varepsilon_0\mu_0}$ is the wave number of the host medium. The presented formulae are valid within the frame of the following approximations: $w, d \ll r$ and the splits of the rings are large enough compared to d . Also, we assume that SRR is formed by ideally conducting rings (no dissipation losses).

The magnetic polarizability (1) takes into account the radiation losses and satisfies to the basic Sipe-Kranendonk condition [1, 26, 30] which in the present case has the following form:

$$\operatorname{Im}(\alpha^{-1}(\omega)) = \frac{k^3}{6\pi\mu_0}. \quad (2)$$

In the following analysis we operate with the inverse polarizability $\alpha^{-1}(\omega)$, thus, we rewrite (1) in the following form:

$$\alpha^{-1}(\omega) = A^{-1} \left(\frac{\omega_0^2}{\omega^2} - 1 \right) + j \frac{k^3}{6\pi\mu_0}. \quad (3)$$

B. Inductively Loaded Short Wires

A typical resonant electric scatterer is an inductively loaded short wire, as shown in Fig. 3.

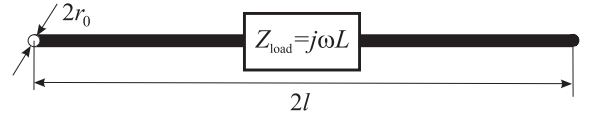


FIG. 3: Geometry of the inductively loaded wire dipole

The electric polarizability α_e of loaded wires following the known model [17] has the form:

$$\alpha_e^{-1} = \frac{3}{l^2 C_{\text{wire}}} \left(\frac{1 - \omega^2/\omega_0^2}{4 - \omega^2/\omega_0^2} \right) + j \frac{k^3}{6\pi\varepsilon_0} \quad (4)$$

where $C_{\text{wire}} = \pi l \varepsilon_0 / \log(2l/r_0)$ is the capacitance of the wire, $\omega_0 = \sqrt{LC_{\text{wire}}}$ is the resonant frequency, L is the inductance of the load, l is the half length of the wire and r_0 is the wire radius.

It is clear, that at the frequencies near the resonance the polarizability of LSW has the form

$$\alpha_e^{-1}(\omega) \approx A_e^{-1} \left(\frac{\omega_0^2}{\omega^2} - 1 \right) + j \frac{k^3}{6\pi\varepsilon_0}, \quad (5)$$

with $A_e = l^2 C_{\text{wire}}$, which is similar to (3). Moreover, if $A_e/\varepsilon_0 = A/\mu_0$ then using duality principle the magnetic dipole with polarizability α (3) can be transformed to the electric dipole with polarizability α_e (3), and vice versa. This means that it is enough to consider only one type of resonant scatterers. In the present paper we have chosen magnetic ones to be principal. The electric scatterers can be easily obtained using duality principle from the magnetic scatterers with $A = \mu_0 A_e/\varepsilon_0$.

III. HOMOGENEOUS MEDIA APPROACH

Let us consider an orthorhombic lattice with periods $a \times b \times c$ formed by magnetic uniaxial scatterers directed along x (see Fig. 1) and described by polarizability (1). For electric scatterers (ILW:s) the problem is dual to the present one. In the long wavelength limit the lattices of scatterers are usually described as homogeneous media with certain material parameters. The lattice under study can be modelled as a resonant uniaxial magnetic. The permeability of such a magnetic is a dyadic of the form:

$$\bar{\mu} = \mu \mathbf{x}_0 \mathbf{x}_0 + \mu_0 (\mathbf{y}_0 \mathbf{y}_0 + \mathbf{z}_0 \mathbf{z}_0).$$

The permeability μ (x -component of the tensor) can be calculated though the individual polarizability of a single scatterer using the Clausius-Mossotti formula [31]:

$$\mu = \mu_0 \left(1 + \frac{\alpha(\omega)/(\mu_0 V)}{1 - C_s(a, b, c) \alpha(\omega)/\mu_0} \right), \quad (6)$$

where $V = abc$ is a volume of the lattice elementary cell and $C_s(a, b, c)$ is the static interaction constant of the lattice. The following expression for this interaction constant is available in [31], p.758:

$$C_s(a, b, c) = \frac{1}{4\pi} \sum_{(m,n,l) \neq (0,0,0)} \frac{2(am)^2 - (bn)^2 - (cl)^2}{[(am)^2 + (bn)^2 + (cl)^2]^{5/2}} \\ = \frac{1.202}{\pi a^3} - \frac{4\pi}{a^3} \sum_{(n,l) \neq (0,0)} \sum_{m=1}^{+\infty} m^2 K_0 \left(\frac{2\pi m}{a} \sqrt{(bn)^2 + (cl)^2} \right), \quad (7)$$

where $K_0(x)$ is the modified Bessel function of 3d kind (the McDonald function). In the case of a cubical lattice $a = b = c$ the interaction constant is equal to the classical value $C_s = 1/(3V)$.

Notice, that the radiation losses contribution in expression (3) should be skipped while substituting into formula (6). This makes permeability purely real number as it should be for lossless regular arrays [1, 26]. This manipulation is based on the fact that the far-field radiation of the single scatterer is compensated by the electromagnetic interaction in a regular three-dimensional array, so that there is no radiation losses for the wave propagating in the lattice. The mathematical proof of this fact

for the general dimensions of lattice is presented in the Appendix.

The typical dependence of magnetic permeability μ on frequency is presented in Fig. 4 for cubic lattice ($a = b = c$) of SRR:s with parameters chosen so that $A = 0.1\mu_0 a^3$ and $\omega_0 = 1/(a\sqrt{\varepsilon_0\mu_0})$. The resonant frequency shift from $ka = 1$ to $ka = 0.984$ is clearly observed. While $ka < 0.984$ the structure is paramagnetic ($\mu > 1$). For ka within $[0.984, 1.0352]$ range the permeability is negative ($\mu < 0$). For $ka > 1.0352$ the medium is diamagnetic ($0 < \mu < 1$).

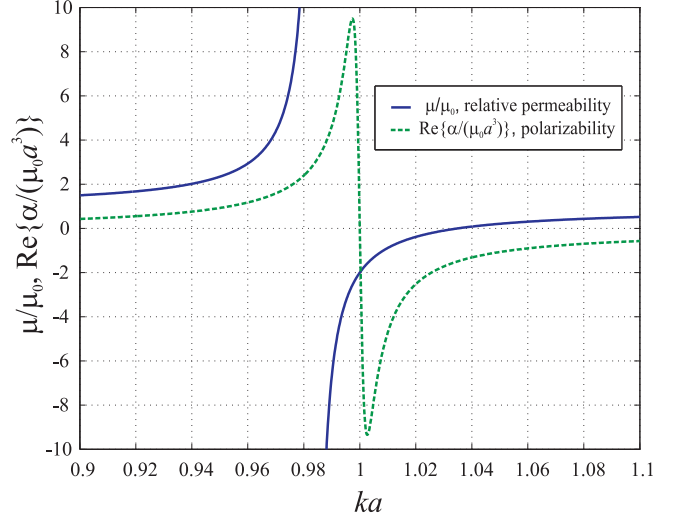


FIG. 4: Dependencies of relative permeability μ/μ_0 and normalized polarizability $\alpha/(\mu_0 a^3)$ vs. normalized frequency ka for cubic lattice ($a = b = c$) of SRR:s with $A = 0.1\mu_0 a^3$ and $\omega_0 = 1/(a\sqrt{\varepsilon_0\mu_0})$.

The dispersion equation for the uniaxial magnetic medium has the following form (see e.g. [24, 25, 31]):

$$\mu_0(q_y^2 + q_z^2) = \mu(k^2 - q_x^2). \quad (8)$$

Thus, the isofrequency surfaces for such material have form of a spheroid if $\mu > 0$ (the spheroid is prolate for $\mu < 1$ and oblate for $\mu > 1$) or a hyperboloid if $\mu < 0$. Both types of isofrequency surfaces have symmetry axis along OX . The media is isotropic in the YZ plane, and we can restrict our consideration by the XY plane without loss of generality. The typical isofrequency contours in this plane are shown in Figs. 5 and 6. The magnetic under consideration has the same parameters as in Fig. 4. The ranges of wave vector components q_x and q_y are restricted by $\pm\pi/a$ and $\pm\pi/b$, respectively, having in mind that the exact dispersion diagram of the lattice corresponds to the first Brillouin zone and we will compare the homogenized model with the exact theory.

While the frequency is below the resonance ($ka < 0.984$) the isofrequency contour has the form of an ellipse prolate along OY ($\mu > 1$). For frequencies above the resonance but less than the frequency at which the permeability turns to zero ($0.984 < ka < 1.0352$) the

To study eigenmodes of the system we introduce the phase distribution of dipole moments determined by the unknown wave vector $\mathbf{q} = (q_x, q_y, q_z)^T$ as follows:

$$M_{m,n,l} = M e^{-j(q_x am + q_y bn + q_z cl)}. \quad (12)$$

Collecting together expressions (9), (11) and (12) we obtain dispersion equation relating the wave vector \mathbf{q} with the frequency ω :

$$M = \alpha \mu_0^{-1} \sum_{(m,n,l) \neq (0,0,0)} G(\mathbf{R}_{m,n,l}) M e^{-j(q_x am + q_y bn + q_z cl)}.$$

It can be rewritten in a more appropriate form:

$$[\mu_0 \alpha^{-1}(\omega) - C(k, \mathbf{q})] M = 0, \quad (13)$$

where

$$C(k, \mathbf{q}, a, b, c) = \sum_{(m,n,l) \neq (0,0,0)} G(\mathbf{R}_{m,n,l}) e^{-j(q_x am + q_y bn + q_z cl)}. \quad (14)$$

We call C as the dynamic interaction constant of the lattice using the analogy with the classical interaction constant from the theory of artificial dielectrics and magnetics [31].

Dispersion equation (13) has two different types of solutions. The first ones are ordinary waves with zero dipole moments ($M = 0$). They are plain waves propagating in the host media which have zero component of magnetic field along direction of dipoles. They do not interact with lattice (do not excite magneto-dipole moments). The waves of second type are extraordinary waves. They excite magneto-dipole moments ($M \neq 0$) strongly interacting with each other. The dispersion equation for extraordinary modes transforms from (13) to

$$\mu_0 \alpha^{-1}(\omega) - C(k, \mathbf{q}, a, b, c) = 0. \quad (15)$$

The solution of this dispersion equation allows to study dispersion diagrams for the crystal under consideration. The main problem is the calculation of the dynamic interaction constant C given by (14). This question is closely related with such concepts as static interaction constant (7) and the triply-periodic dyadic Green's function. The static interaction constant can be obtained from (14) by letting $k = q_x = q_y = q_z = 0$ and choosing appropriate order of summation for obtained conditionally convergent series [32]. The plane-wise summation method [32, 33] or Poisson summation formulae based technique [31, 34] are usually applied for calculation of the static interaction constant. The triply-periodic dyadic Green's function represents the field produced by a phased lattice of point dipoles. If the zero-numbered term is added to series (14) (simultaneously one should move the observation point in (10) from the node of the lattice to avoid singularity) formula (14) will give a co-polarized component of the dyadic Green's function. The triply-periodic dyadic Green's function is usually evaluated with help

of classical Ewald's method [35–37]. However, the other methods of summation (with improved convergence rate) exist as well [38, 39]. All the listed above methods can be applied for evaluation of dynamic interaction constant (14). The Ewald's method require an appropriate choice of a splitting parameter [40], which is a sophisticated manipulation. Also, it does not show the energy balance in the lattice (as well as other methods mentioned above). Therefore, we have chosen an original method of summation. Our approach combines the plane-wise summation [32, 33] and the Poisson summation technique with singularity cancellation [31]. The details of the evaluation of C which includes the energy balance condition as an intermediate step are presented in Appendix.

V. DISPERSION PROPERTIES OF THE CRYSTAL

The dispersion equation (15) with interaction constant $C(k, \mathbf{q})$ given by formula (A37) from Appendix is solved numerically. The parameters of the structure are the same as those of the homogenized structure: cubic lattice ($a = b = c$) of SRR:s, $A = 0.1 \mu_0 a^3$ and $\omega_0 = 1/(a \sqrt{\varepsilon_0 \mu_0})$. The dispersion diagram for the crystal is presented in Fig. 7. The points $\Gamma = (0, 0, 0)^T$, $X = (\pi/a, 0, 0)^T$, $Y = (0, \pi/a, 0)^T$, $L = (0, \pi/a, \pi/a)^T$, $K = (\pi/a, 0, \pi/a)^T$ and $R = (\pi/a, \pi/a, \pi/a)^T$ of the first Brillouin zone are illustrated at the sketch in the left bottom corner of the plot. The dotted lines represent dispersion curves for ordinary modes of the crystal which coincide with light lines. The incomplete resonant stop band for extraordinary modes (similar to discussed in [26]) is observed in vicinity of the resonance of individual inclusions.

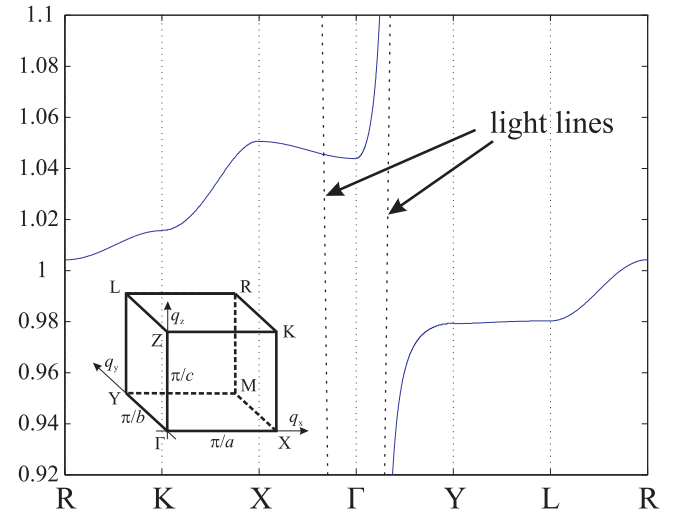


FIG. 7: Dispersion diagram for cubic lattice ($a = b = c$) of SRR:s with $A = 0.1 \mu_0 a^3$ and $\omega_0 = 1/(a \sqrt{\varepsilon_0 \mu_0})$.

The dispersion curve for (010) direction (branch ΓY in Fig. 7) is shown in Fig. 8 for comparison with result predicted by homogenization model. For this direction of

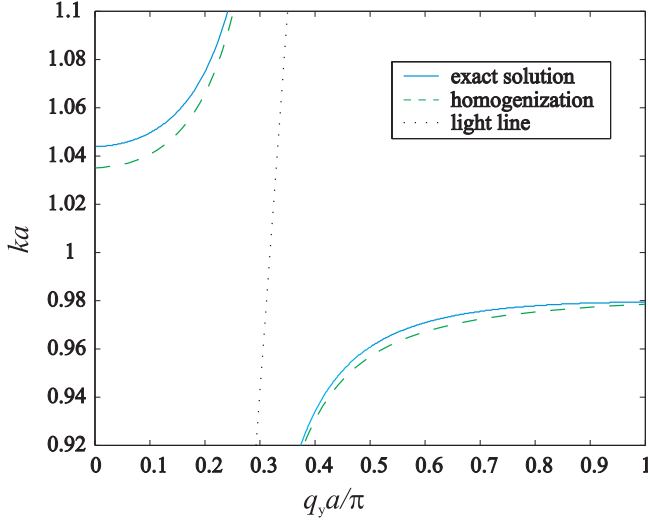


FIG. 8: Dispersion curve for (010) direction. Exact solution (solid line), prediction by homogenization model (dashed line) and light line (dotted line).

propagation the agreement with the homogenized model is fine except narrow frequency range $ka \approx 0.98$. This region is not visible in Fig. 8 but it is clear from Fig. 7 that this is the lower edge of the stop-band for waves propagating in the transverse plane (YZ). This frequency range in the homogenization model corresponds to high propagation constant $q_y > \pi/a$ and high positive permeability $\mu > \pi^2/(ka)^2$. This means that the homogenization in the case $\mu > \pi^2/(ka)^2$, strictly speaking, describes the dispersion of the lattice in a wrong manner. This is an expected result which corresponds to the known predictions of the classical theory [1]. Below we will consider this frequency range in details.

The frequency band $0.9803 < ka < 1.044$ corresponds to the negative axial permittivity of the homogenized model of the lattice. Negative axial permittivity means the imaginary propagation constant for the transverse plane and this result nicely corresponds to the stop-band for the YZ plane predicted by the exact theory. So, the homogenization within $0.9803 < ka < 1.044$ is allowed.

The isofrequency contours in YZ plane for frequencies near the bottom $ka = 0.96 \dots 0.9803$ and top $ka = 1.04 \dots 1.10$ edges of the transverse stop band are presented in Fig. 9. The behavior of isofrequency contours shown in Fig. 9 is typical for general electromagnetic crystals at the frequencies near the stop band edges [41–43]. While the frequency is rather far below the stop band ($ka < 0.979$) the isofrequency contours have form of circles and the agreement with the homogenized model is fine. The same behavior is observed above the stop band ($ka > 1.044$). The circles for $ka > 1.044$ are smaller than those for $ka < 0.979$ which nicely corresponds to the smaller effective permeability (see Fig. 4). However, within the narrow frequency range $0.979 < ka < 0.9803$ the isofrequency contours acquire a form which is differ-

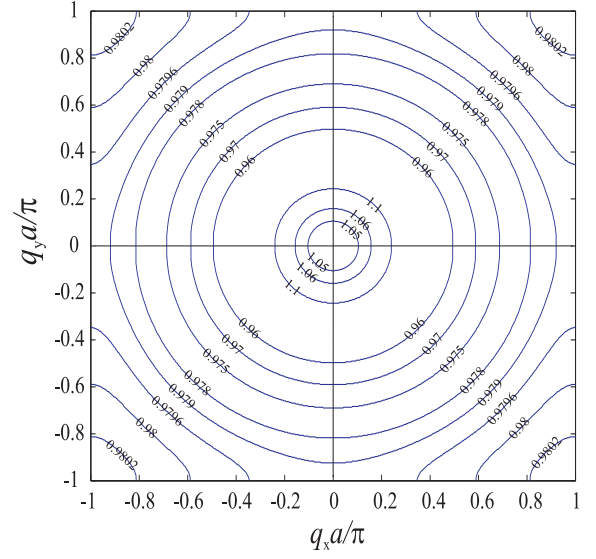


FIG. 9: Isofrequency contours in YZ plane for frequencies near of the bottom edge of stop band.

ent from a circle. This anisotropy in the transverse plane gives the evidence of spatial dispersion. Notice, that in this band in the lattice there are two evanescent modes whose wave vectors lie in the transverse plane (see also [26]). Strictly speaking, the crystal can not be homogenized at these frequencies. And these frequencies correspond to high positive μ of the homogenized lattice. It was already noticed above that it is the expected result.

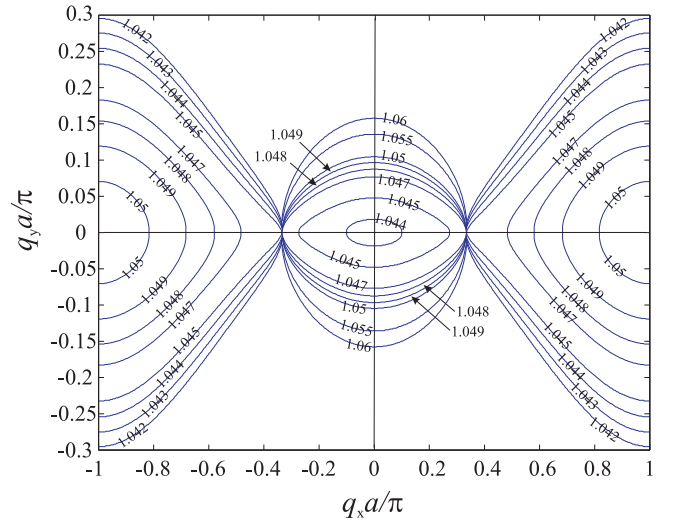


FIG. 10: Isofrequency contours in XY plane for frequencies near the top edge of stop band.

Significant disagreement between the exact solution and the result of homogenization was also obtained at the frequencies near the top edge of the stop band. The isofrequency contours in XY plane for this frequency range are presented in Fig. 10. They dramatically differs from prediction given by homogenization model shown

in Fig. 6. Following to homogenization approach, the isofrequency contours should have hyperbolic form at the frequencies corresponding to negative effective permittivity and elliptic one in the case of positive permittivity (see Fig. 6). The exact modeling reveals that this switching between hyperbolic and elliptic types of isofrequency contours happens in the different manner. While $ka < 1.0435$ the isofrequency contours has a form which is similar to hyperbolic one but they are already distorted. At the higher frequencies $ka > 1.0435$ the ‘hyperbolic’ contours continue to distort, and simultaneously the ‘elliptic’ contours (the second branch of the same isofrequency) appear in vicinity of Γ point. The ‘hyperbolic’ contours pass through points $q_x = \pm k$ while $ka < 1.0455$, but ‘elliptic’ ones do not. For $ka > 1.046$ the situation changes to the opposite one. The ‘elliptic’ contours acquire fixed size along OX axis and starts to pass through points $q_x = \pm k$. On the other hand, the ‘hyperbolic’ contours start to collapse around X-point and completely disappear for $ka > 1.051$. This way the ‘hyperbolic’ contours transform to ‘elliptic’ ones passing through the regime where both types of contours co-exist at the same frequencies. At any frequency only one of these contours passes through points $q_x = \pm k$.

Thus, in the region $1.043 < ka < 1.051$ the homogenization gives wrong results for the waves propagating in the XY plane because of the two-mode regime observed in original structure. This region corresponds to the small absolute values of μ ($|\mu| < 0.2$ in our case). Strictly speaking, the homogenization in the region of small $|\mu|$ turns out to be forbidden. In our opinion, this is a qualitatively new result. However, as it follows from Fig. 9 the homogenized model makes correct prediction for the waves propagating in the YZ plane in the band $1.043 < ka < 1.051$. One can conclude that the homogenization at these frequencies (forbidden in its strict meaning) is however allowed for a case of transversal propagation.

The described regime of the co-existence of ‘hyperbolic’ and ‘elliptic’ isofrequency contours at a fixed frequency means the bi-refringence for extraordinary modes and three-refringence in the case of the refraction (one ordinary wave and two extraordinary ones). An extraordinary mode corresponding to the ‘hyperbolic’ contour refracts negatively, and the other one (corresponding to the ‘elliptic’ contour) experiences positive refraction. This property can find different applications (beam splitting, etc).

VI. CANALIZATION REGIME AND SUBWAVELENGTH IMAGING

Above, we pointed out that near the bottom edge of the stop-band (frequencies corresponding to high positive μ) the homogenized model wrongly predicts the dispersion of the waves propagating in the YZ plane. Now let us show that the homogenized model gives the qualitatively

correct predictions in this frequency region if consideration is restricted by the propagation in the XY plane. The isofrequency contours in XY plane for frequencies near bottom edge of stop band are presented in Fig. 11. The behavior of contours is in the good agreement with the predictions of the homogenized model (see Fig. 5). The difference is noticed only near the edges of the lowest Brillouin zone. So, the homogenization (forbidden in its strict meaning for $ka \approx 0.98$) is still allowed for a case of oblique propagation with respect to the optical axis.

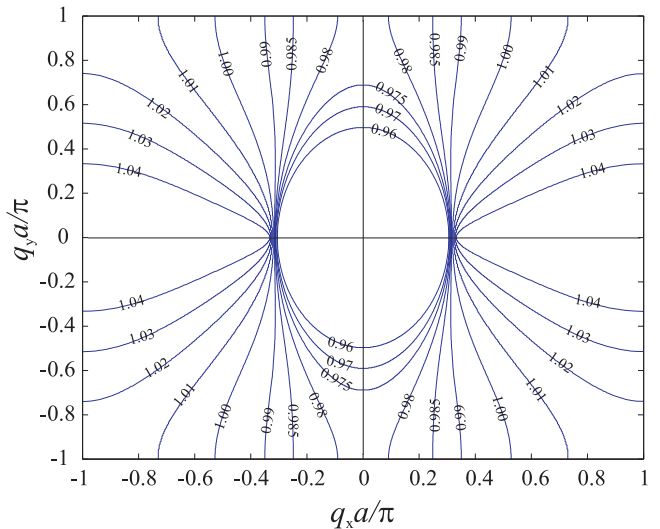


FIG. 11: Isofrequency contours in XY plane for frequencies near the bottom edge of stop band.

At the frequencies near $ka = 0.989$ the isofrequency contours are practically flat. It means that all eigenmodes at such frequencies have the same axial component $q_x = \pm k$ of the wave vector. Moreover, they all have the same group velocity (the group velocity is normal to the isofrequency contour). This makes the eigenmode to be the so-called transmission line mode like that of the wire medium [16]. For both lattice of uniaxial scatterers and wire medium this isofrequency corresponds to the infinite material parameter of the homogenized model. The difference is that in the present case the flat isofrequency contour exists at a single frequency $ka = 0.989$ in contrast to wire medium which support transmission line modes in a very wide frequency range.

The flat isofrequency contour we found can be used for the implementation of the so-called canalization regime described in our recent paper [43]. The similar regimes are called also as self-guiding [44], directed diffraction [45], self-collimation [46] and tunneling [47]. In [43] we have shown that not only all plane waves are collimated into a strictly parallel beam at the flat isofrequency. All evanescent waves impinging the medium at this frequency will be also transformed into the plane wave with $q_x = k$ transporting the energy along the optical axis. Therefore this regime allows to create subwavelength images of the sources and transmit their near field to unre-

stricted distances.

The canalization regime for a slab of the medium possessing the flat isofrequency does not involve negative refraction and amplification of evanescent modes which are usually used for that purpose [8, 42, 48]. Its main feature is transformation of the spatial spectrum of the incident field into a collimated beam directed across the slab. All spatial harmonics of the source refract into such the eigenmodes at the front interface. These eigenmodes all propagate normally to the interface with same velocity and deliver the input distribution of electric field to the back interface. Their refraction at the back interface forms the image. The problem of the reflection from a slab (and inner reflections in the slab) can be solved using the Fabry-Pérot resonance. The Fabry-Pérot resonance holds for all incidence angles including the complex angles. The reason of that is simple: after the refraction all the incident waves acquire the same longitudinal component of the wave vector $q_x = k$. Thus, in the canalization regime there is no image deterioration by the finite thickness of the lens (there are no waves travelling along the interfaces).

VII. CONCLUSION

In the present paper we have studied dispersion properties of the electromagnetic crystals formed by uniaxial resonant scatterers (magnetic and electric ones). The structures are modelled using the local field approach. The main tricky point of this theory is evaluating the dynamic interaction constant of the lattice. This constant has been calculated using a special analytical method based on the plane-wise summation approach, Poisson summation formula, singularity cancellation technique and convergence acceleration of slowly convergent series. As a result, a transcendental dispersion equation has been obtained in the form suitable for rapid and efficient numerical calculations. The comparison of exact solution provided by this equation with homogenization

model allows to show that the structure, strictly speaking, can not be homogenized not only at the frequencies which correspond to the very high values of effective permeability or permittivity (this was well known earlier) but also at the frequencies corresponding to small absolute values of them.

However, if one is interested in a special cases of propagation then the homogenization can be allowed in both these frequency bands. For the propagation in the plane comprising the optical axis the homogenization is allowed in the region of large material parameters. For the propagation in the plane orthogonal to the optical axis the homogenization is allowed in the region of small material parameters.

During this study we have found two interesting properties of the crystals under consideration. At a single frequency near the bottom edge of stop band the isofrequency contour is flat and this frequency corresponds to the infinite permeability or permittivity. This fact makes possible to use the crystals for subwavelength imaging. The two-mode regime is observed at frequencies near the top edge of stop band. This corresponds to the bi-refrindex for extraordinary waves and to three-refrindex of the incident wave in the general case of arbitrary polarization, which can be used for beam splitting.

The dispersion theory presented in this paper is a powerful tool for dispersion analysis of three-dimensional electromagnetic crystals. In the present form the theory is restricted to the case of simple (uniaxial) scatterers, but it can be extended to the case of electric or magnetic scatterers with arbitrary dyadic response. This will be done in our future publications. In this case it will be possible to develop an analytical theory for a lattice of the isotropic resonant scatterers (e.g. metallic spheres in the optical range) in more accurate manner than the known low-frequency approximations [31, 34, 35, 49] allow to do. This can be actual for the optics of metal nano-particles which is developing fast.

-
- [1] J. Sipe and J. V. Kranendonk, Phys. Rev. A **9**, 1806 (1974).
 - [2] A. Serdyukov, I. Semchenko, S. Tretyakov, and A. Sihvola, *Electromagnetics of bi-anisotropic materials: Theory and applications* (Amsterdam: Gordon and Breach Science Publishers, 2001).
 - [3] I. Lindell, A. Sihvola, S. Tretyakov, and A. Viitanen, *Electromagnetic Waves and Bi-Isotropic Media* (Boston, MA: Artech House Publishers, 1994).
 - [4] S. Ponti, J. Reyes, and C. Oldano, J. Phys.: Condens. Matter **14**, 10173 (2002).
 - [5] W. Weber and G. Ford, Phys. Rev. B **70**, 125429 (2004).
 - [6] A. Alu, A. Salandrino, and N. Engheta, arXiv: cond-mat/0412263 (2005).
 - [7] V. Veselago, Sov. Phys. Usp. **10**, 509 (1968).
 - [8] J. Pendry, Phys. Rev. Lett. **85**, 3966 (2000).
 - [9] D. R. Smith, W. J. Padilla, D. C. Vier, S. C. Nemat-Nasser, and S. Schultz, Phys. Rev. Lett. **84**, 4184 (2000).
 - [10] R. A. Shelby, D. R. Smith, and S. Schultz, Science **292**, 77 (2001).
 - [11] A. Houck, J. Brock, and I. Chuang, Phys. Rev. Lett. **90**, 137401 (2003).
 - [12] J. Brown, Progress in dielectrics **2**, 195 (1960).
 - [13] W. Rotman, IRE Trans. Ant. Propag. **10**, 82 (1962).
 - [14] J. Pendry, A. Holden, W. Steward, and I. Youngs, Phys. Rev. Lett. **76**, 4773 (1996).
 - [15] J. Pendry, A. Holden, D. Robbins, and W. Stewart, IEEE Trans. Microwave Theory Techn. **47**, 2075 (1999).
 - [16] P. Belov, R. Marques, S. Maslovski, I. Nefedov, M. Silveirinha, C. Simovski, and S. Tretyakov, Phys. Rev. B **67**, 113103 (2003).
 - [17] S. Tretyakov, S. Maslovski, and P.A. Belov, IEEE Trans.

- Antennas Propagat. **51**, 2652 (2003).
- [18] R. Ziolkowski, IEEE Trans. Antennas Propag. **51**, 1516 (2003).
 - [19] C. Simovski and S. He, Phys. Lett. A **311**, 254 (2003).
 - [20] E. Verney, B. Sauviac, and C. Simovski, Phys. Lett. A **331**, 244 (2004).
 - [21] D. R. Smith and D. Schurig, Phys. Rev. Lett. **90**, 077405 (2003).
 - [22] D. R. Smith, P. Kolinko, and D. Schurig, J. Opt. Soc. Am. B **21**, 1032 (2004).
 - [23] D. R. Smith, D. Schurig, J. J. Mock, P. Kolinko, and P. Rye, Appl. Phys. Lett. **84**, 2244 (2004).
 - [24] I. Lindell, S. Tretyakov, K. Nikoskinen, and S. Ilvonen, Microw. Optical Technology Lett. **31**, 129 (2001).
 - [25] P. Belov, Microw. Optical Technology Lett. **37**, 259 (2003).
 - [26] P. Belov, S. Tretyakov, and A. Viitanen, Phys. Rev. E **66**, 016608 (2002).
 - [27] R. Marques, F. Medina, and R. Rafii-El-Idrissi, Phys. Rev. B **65**, 144440 (2002).
 - [28] B. Sauviac, C. Simovski, and S. Tretyakov, Electromagnetics **24**, 317 (2004).
 - [29] C. Simovski, P.A.Belov, and S. He, IEEE Trans. Antennas Propagat. **51**, 2582 (2003).
 - [30] P. Belov, S. Maslovski, C. Simovski, and S. Tretyakov, Technical Physics Letters **29**, 36 (2003).
 - [31] R. Collin, *Field Theory of Guided Waves* (IEEE Press, Piscataway, NJ, 1990).
 - [32] B. Nijboer and F. de Wette, Physica **24**, 422 (1958).
 - [33] F. de Wette and G. Schacher, Phys. Rev. **137**, 78 (1965).
 - [34] M. Kharadly and W. Jackson, Proc. IEE **100**, 199 (1962).
 - [35] P. P. Ewald, Ann. Der Phys. **64**, 253287 (1921).
 - [36] M. G. Silveirinha and C. A. Fernandes, IEEE Trans. Microw. Theory Techn. **53**, 347 (2005).
 - [37] M. G. Silveirinha and C. A. Fernandes, IEEE Trans. Microw. Theory Techn. **52**, 889 (2004).
 - [38] N. Nicorovich, R. McPhedran, and B. Ke-Da, Phys. Rev. E **51**, 690 (1995).
 - [39] A. Borji and S. Safavi-Naeni, IEEE Trans. Microw. Theory Techn. **52**, 1724 (2004).
 - [40] A. Kustepeli and A. Martin, IEEE Microwave Guided Wave Lett. **10**, 168 (2000).
 - [41] M. Notomi, Phys. Rev. B **62**, 10696 (2000).
 - [42] C. Luo, S. G. Johnson, J. D. Joannopoulos, and J. B. Pendry, Phys. Rev. B **65**, 201104 (2002).
 - [43] P. Belov, C. Simovski, and P. Ikonen, submitted to Phys. Rev. B (2005).
 - [44] D. N. Chigrin, S. Enoch, C. M. S. Torres, and G. Tayeb, Optics Express **11**, 1203 (2003).
 - [45] H.-T. Chien, H.-T. Tang, C.-H. Kuo, C.-C. Chen, and Z. Ye, Phys. Rev. B **70**, 113101 (2004).
 - [46] Z.-Y. Li and L.-L. Lin, Phys. Rev. B **68**, 245110 (2003).
 - [47] C.-H. Kuo and Z. Ye, Phys. Rev. E **70**, 056608 (2004).
 - [48] C. Luo, S. G. Johnson, J. D. Joannopoulos, and J. B. Pendry, Phys. Rev. B **68**, 045115 (2003).
 - [49] E. Smith, J. Phys. A: Math. Gen. **13**, L107 (1980).
 - [50] P. Belov, S. Tretyakov, and A. Viitanen, J. Electromagn. Waves Applic. **16**, 1153 (2002).
 - [51] L. Kantorovich and V. Krylov, *Approximate Methods of Higher Analysis* (Intersc. Publish. Inc., NY, 1958).
 - [52] S. Tretyakov and A. Viitanen, Electrical Engineering **82**, 353 (2000).

APPENDIX A: EVALUATION OF DYNAMIC INTERACTION CONSTANT

For calculation of the dynamic interaction constant $C(k, \mathbf{q})$ (14) we apply a method based on plane-wise summation, Poisson summation formulae and singularity cancellation technique. This method was applied in [50] for calculation of the two-dimensional dynamic interaction constant for theory of doubly-periodic wire lattices. The series in (14) are divergent in classical meaning, but the physical reasoning of necessary type of summation is clear enough. Due to existence of losses in real space one should add infinitesimal imaginary part to the wave vector k of free space and tend it to zero in order to get the correct result.

We split series (14) (remember that the zero term is excluded from summation) onto three parts:

$$\sum_{l \neq 0} \sum_{m=-\infty}^{+\infty} \sum_{n=-\infty}^{+\infty} + \sum_{n \neq 0} \sum_{m=-\infty}^{+\infty} \left|_{l=0} \right. + \sum_{m \neq 0} \left|_{l=n=0} \right.$$

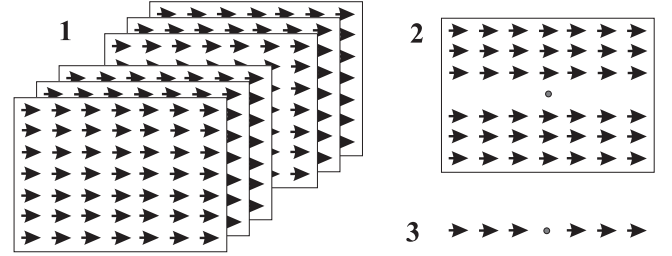


FIG. 12: Splitting areas

These parts are denoted as $C_{1,2,3}$ respectively, and $C = C_1 + C_2 + C_3$. The splitting areas are shown in Fig.12. The term C_1 describes contribution into the local field from all plane grids which are parallel to the OXY plane except the grid located at this plane. The term C_2 corresponds to the contribution of the dipole linear chains parallel to the OX axis and located at OXY plane except the chain located at this axis. The term C_3 is the contribution from all dipoles of the chain located at the OX axis except the dipole located at the origin of coordinate system. Notice, that $C_2 + C_3$ gives the interaction constant of the planar grid.

For evaluation of the term C_1 it is possible to use the Poisson summation formula for double series which leads to the expression with rapidly (exponentially) convergent series. The term C_2 can be calculated using the ordinary Poisson summation formula together with the singularity cancellation technique [31]. It is impossible to apply Poisson summation formula for evaluation of the term C_3 since it contain non-complete series. Convergence of these series can be accelerated using the dominant part extraction [51].

1. Contribution of parallel planar grids

The double Fourier transformation of any function $f(x, y)$ is defined as follows:

$$F(p, q) = \mathbf{L}_{x,y} \{f(x, y)\} = \int_{-\infty}^{+\infty} \int_{-\infty}^{+\infty} f(x, y) e^{-j(px+qy)} dx dy.$$

The Poisson summation formula for double series has the following form: [31]:

$$\sum_{m=-\infty}^{+\infty} \sum_{n=-\infty}^{+\infty} f(am, bn) = \frac{1}{ab} \sum_{m=-\infty}^{+\infty} \sum_{n=-\infty}^{+\infty} F\left(\frac{2\pi m}{a}, \frac{2\pi n}{b}\right). \quad (\text{A1})$$

The double Fourier transform of the Hertz potential of a dipole reads as:

$$\mathbf{L}_{x,y} \left\{ \frac{1}{4\pi} \frac{e^{-jk\sqrt{x^2+y^2+z^2}}}{\sqrt{x^2+y^2+z^2}} \right\} = \frac{1}{2} \frac{e^{-|z|\sqrt{p^2+q^2-k^2}}}{\sqrt{p^2+q^2-k^2}}, \quad (\text{A2})$$

where the sign of square root should be chosen so that $\text{Im}(\sqrt{p^2+q^2-k^2}) \geq 0$.

Applying the shift and differential properties of Fourier transformation to the Fourier-image of the Hertz potential (A2) we obtain the transformation rule:

$$\begin{aligned} \mathbf{L}_{x,y} \left\{ \left[\left(k^2 + \frac{\partial^2}{\partial x^2} \right) \frac{e^{-jk\sqrt{x^2+y^2+z^2}}}{\sqrt{x^2+y^2+z^2}} \right] \frac{e^{-j(q_x x + q_y y)}}{4\pi} \right\} \\ = \frac{k^2 - (q_x + p)^2}{2} \frac{e^{-|z|\sqrt{(q_x+p)^2+(q_y+q)^2-k^2}}}{\sqrt{(q_x+p)^2+(q_y+q)^2-k^2}}, \quad (\text{A3}) \end{aligned}$$

Using the Poisson summation formula (A1) together with (A3) we obtain the term C_1 in the form:

$$C_1 = \sum_{l \neq 0} \sum_{m=-\infty}^{+\infty} \sum_{n=-\infty}^{+\infty} \frac{jp_m^2}{2ab} \frac{e^{-j(|cl|k_z^{(mn)}+q_z cl)}}{k_z^{(mn)}}, \quad (\text{A4})$$

where

$$k_x^{(m)} = q_x + \frac{2\pi m}{a}, \quad k_y^{(n)} = q_y + \frac{2\pi n}{b},$$

$$p_m = \sqrt{\left(k_x^{(m)}\right)^2 - k^2},$$

$$k_z^{(mn)} = -j \sqrt{\left(k_x^{(m)}\right)^2 + \left(k_y^{(n)}\right)^2 - k^2}.$$

Here we choose $\text{Im}(\sqrt{\cdot}) \geq 0$, so that $\text{Im}(k_z^{(mn)}) \leq 0$. The representation (A4) can be treated as an expansion

of the fields produced by parallel dipole grids in terms of the Floquet modes. The wave vectors of these modes are

$$\mathbf{k}^{(mn)} = \left(k_x^{(m)}, k_y^{(n)}, k_z^{(mn)} \right)^T.$$

The series by l index in (A4) are geometrical progressions and their summation can be made directly:

$$\sum_{l \neq 0} e^{-j(|cl|k_z^{(mn)}+q_z cl)} = -\frac{e^{-jk_z^{(mn)}c} - \cos q_z c}{\cos k_z^{(mn)}c - \cos q_z c}.$$

It allows to rewrite expression (A4) for the term C_1 as

$$C_1 = \sum_{m=-\infty}^{+\infty} \sum_{n=-\infty}^{+\infty} \frac{p_m^2}{2jabk_z^{(mn)}} \frac{e^{-jk_z^{(mn)}c} - \cos q_z c}{\cos k_z^{(mn)}c - \cos q_z c}. \quad (\text{A5})$$

These series possess exponential convergence. It is clearly seen if the second factor of the term under sign of the sum in (A5) is rewritten as

$$-\left[\frac{1}{e^{j(k_z^{(mn)}+q_z)c} - 1} + \frac{1}{e^{j(k_z^{(mn)}-q_z)c} - 1} \right].$$

This makes (A5) suitable for rapid numerical calculations.

2. Contribution of parallel chains from OXY-plane

The ordinary Fourier transformation has the form

$$F(p) = \mathbf{L}_x \{f(x)\} = \int_{-\infty}^{+\infty} f(x) e^{-jpx} dx.$$

Poisson's summation formula for single series reads:

$$\sum_{m=-\infty}^{+\infty} f(am) = \frac{1}{a} \sum_{m=-\infty}^{+\infty} F\left(\frac{2\pi m}{a}\right). \quad (\text{A6})$$

The Fourier transform for the Hertz's potential of a dipole is following:

$$\mathbf{L}_x \left\{ \frac{1}{4\pi} \frac{e^{-jk\sqrt{x^2+y^2+z^2}}}{\sqrt{x^2+y^2+z^2}} \right\} = \frac{1}{2\pi} K_0 \left(\sqrt{p^2 - k^2} \sqrt{y^2 + z^2} \right). \quad (\text{A7})$$

Thus, applying shift and differential properties of Fourier transformation to the image of Hertz's potential (A7) we get the following transformation rule:

$$\begin{aligned} \mathbf{L}_x \left\{ \frac{1}{4\pi} \left(k^2 + \frac{\partial^2}{\partial x^2} \right) \frac{e^{-jk\sqrt{x^2+y^2+z^2}}}{\sqrt{x^2+y^2+z^2}} \right\} \\ = \frac{1}{2\pi} (k^2 - p^2) K_0 \left(\sqrt{p^2 - k^2} \sqrt{y^2 + z^2} \right). \quad (\text{A8}) \end{aligned}$$

Using Poisson's summation formulae (A6) together with (A8) we obtain the term C_2 in the form:

$$C_2 = - \sum_{n \neq 0} \sum_{m=-\infty}^{+\infty} \frac{p_m^2}{2\pi a} K_0(p_m |bn|) e^{-jq_y bn}. \quad (\text{A9})$$

If arguments of McDonald's functions in (A9) have nonzero real part then the series by index n have very good convergence, but if these are getting imaginary then McDonald's functions transform to Hankel's functions and the mentioned series become slowly convergent. Therefore we separate the part of (A9) which has good convergence:

$$C'_2 = - \sum_{n=1}^{+\infty} \sum_{\text{Re}(p_m) \neq 0} \frac{p_m^2}{\pi a} K_0(p_m bn) \cos(q_y bn). \quad (\text{A10})$$

The residuary part of (A9) ($C'_2 = C'_2 + C''_2$)

$$C''_2 = - \sum_{n \neq 0} \sum_{\text{Re}(p_m)=0} \frac{p_m^2}{2\pi a} K_0(p_m |bn|) e^{-jq_y bn}, \quad (\text{A11})$$

which has slow convergence should be calculated with help of special method. Note, that there is only finite number of indexes m such that $\text{Re}(p_m) = 0$. It means that in (A11) the summation by index m includes only finite number of terms. For example, at the low frequency limit, when period a is large compared with wavelength in the host media, the equation $\text{Re}(p_m) = 0$ has only one solution $m = 0$ if $q_x < k$.

We will calculate the sum of the series (A11) as the limit with z tending to zero:

$$C''_2 = \lim_{z \rightarrow 0} \sum_{n \neq 0} \sum_{\text{Re}(p_m)=0} \frac{-p_m^2}{2\pi a} K_0\left(p_m \sqrt{(bn)^2 + z^2}\right) e^{-jq_y bn}. \quad (\text{A12})$$

Introducing the auxiliary parameter z makes possible to complement series (A12) by zeroth terms and then to use the Poisson summation formula by index n (see (A3) for necessary Fourier transform). The result is as follows:

$$C''_2 = \lim_{z \rightarrow 0} \sum_{\text{Re}(p_m)=0} \frac{-p_m^2}{2ab} \left(\sum_{n=-\infty}^{+\infty} \frac{e^{-j|z|k_z^{(mn)}}}{jk_z^{(mn)}} - \frac{b}{\pi} K_0(p_m |z|) \right) \quad (\text{A13})$$

The term $K_0(p_m |z|)$ in (A13) plays role of the zero term which is subtracted from the complete series (already transformed using Poisson summation formula) in order to get series (A12) without zero term. This term contains singularity if z tends to zero. This singularity disappears in (A13) during subtraction from the complete series which experience the same singularity. In order to cancel out these singularities analytically we apply the method of a dominant series. Namely, we split the series from (A13) onto dominant and correction parts:

$$\sum_{n=-\infty}^{+\infty} \frac{e^{-j|z|k_z^{(mn)}}}{jk_z^{(mn)}} = 2b \sum_{n=1}^{+\infty} \frac{e^{-2\pi|z|n/b}}{2\pi n}$$

$$+ \sum_{n \neq 0} \left[\frac{e^{-j|z|k_z^{(mn)}}}{jk_z^{(mn)}} - b \frac{e^{-2\pi|z|n/b}}{2\pi|n|} \right] + \frac{e^{-j|z|k_z^{(m0)}}}{jk_z^{(m0)}}.$$

The dominant series can be evaluated using the tabulated formula (see [31], Appendix):

$$\sum_{n=1}^{+\infty} \frac{e^{-n\alpha}}{n} = -\log(1 - e^{-\alpha}). \quad (\text{A14})$$

The whole singularity is included into the dominant series. The correction series have no singularity when z tends to zero. Using this fact the formula (A13) can be rewritten as:

$$C''_2 = \sum_{\text{Re}(p_m)=0} \frac{-p_m^2}{2ab} \left(\frac{1}{jk_z^{(m0)}} + \sum_{n \neq 0} \left[\frac{1}{jk_z^{(mn)}} - \frac{b}{2\pi|n|} \right] - \frac{b}{\pi} \lim_{z \rightarrow 0} \left[\log(1 - e^{-2\pi|z|/b}) + K_0(p_m |z|) \right] \right) \quad (\text{A15})$$

The logarithmic singularity occurring here is compensated by that arising from the term with the McDonald function. The small-argument expression for the McDonald function reads:

$$K_0(\alpha) \rightarrow -[\gamma + \log(\alpha/2)],$$

where $\gamma = 0.577$ is Euler's constant.

Thus, the value of the limit in (A15) is as follows:

$$\lim_{z \rightarrow 0} [\cdot] = - \left(\log \frac{b|p_m|}{4\pi} + \gamma + j \frac{\pi}{2} \right). \quad (\text{A16})$$

The series in (A15) with index $n \in [-\infty, +\infty]$ except $n = 0$ have convergence $1/n^2$. Such convergence rate makes calculations not rapid enough. the convergence can be accelerated by extraction of the dominant series. In order to get the convergence $1/n^4$ it is enough to extract series of order $1/n^2$ and $1/n^3$:

$$\sum_{n=1}^{+\infty} \left[\frac{1}{jk_z^{(m,n)}} - \frac{b}{2\pi n} \right] = \sum_{n=1}^{+\infty} \left[\frac{1}{jk_z^{(m,n)}} - \frac{b}{2\pi n} + \frac{q_y b^2}{4\pi^2 n^2} - \frac{l_m b^3}{16\pi^3 n^3} \right] - \frac{q_y b^2}{24} + 1.202 \frac{l_m b^3}{16\pi^3}, \quad (\text{A17})$$

where $l_m = 2q_y^2 - p_m^2$ and we have taken into account, that

$$\sum_{n=1}^{+\infty} \frac{1}{n^2} = \frac{\pi^2}{6}, \quad \sum_{n=1}^{+\infty} \frac{1}{n^3} = 1.202.$$

Collecting the terms corresponding to $+n$ and $-n$ together in (A15) we obtain:

$$\sum_{n \neq 0} \left[\frac{1}{jk_z^{(mn)}} - \frac{b}{2\pi|n|} \right] = \sum_{n=1}^{+\infty} \left[\frac{1}{jk_z^{(m,n)}} + \frac{1}{jk_z^{(m,-n)}} - \frac{b}{\pi n} \right] \quad (\text{A18})$$

$$= \sum_{n=1}^{+\infty} \left[\frac{1}{jk_z^{(m,n)}} + \frac{1}{jk_z^{(m,-n)}} - \frac{b}{\pi n} - \frac{l_m b^3}{8\pi^3 n^3} \right] + 1.202 \frac{l_m b^3}{8\pi^3}.$$

The property $k_z^{(m,-n)}(q_x, q_y) = k_z^{(m,n)}(q_x, -q_y)$ makes function

$$\frac{1}{jk_z^{(m,n)}} + \frac{1}{jk_z^{(m,-n)}} =$$

$$\left[\frac{\frac{b}{2\pi|n|}}{\sqrt{\left(\frac{q_y b}{2\pi n} + 1\right)^2 + \frac{p_m^2}{4\pi^2 n^3/b^2}}} + \frac{\frac{b}{2\pi|n|}}{\sqrt{\left(\frac{q_y b}{2\pi n} - 1\right)^2 + \frac{p_m^2}{4\pi^2 n^3/b^2}}} \right]$$

even with respect to variable $q_y b/(2\pi n)$. It means that being expanded into Taylor series it will contain only even power terms. Thus, the transformed series (A18) being expanded as the series of the order $1/n$ will contain only odd-power terms. In (A18) we have already extracted the dominant series of the order $1/n^3$. So, we conclude that series (A18) have convergence of the order $1/n^5$ which is better than it was estimated when we started to extract dominant series in (A17)

Collecting the parts of the term C_2 given by (A10), (A15), (A16) and (A18) we obtain the final formula for C_2 possessing convergence which is appropriate for rapid and effective numerical calculations:

$$C_2 = - \sum_{n=1}^{+\infty} \sum_{\text{Re}(p_m) \neq 0} \frac{p_m^2}{\pi a} K_0(p_m b n) \cos(q_y b n),$$

$$- \sum_{\text{Re}(p_m)=0} \frac{p_m^2}{2ab} \left(\frac{1}{jk_z^{(m,0)}} + \sum_{n=1}^{+\infty} \left[\frac{1}{jk_z^{(m,n)}} + \frac{1}{jk_z^{(m,-n)}} \right. \right.$$

$$\left. \left. - \frac{b}{\pi n} - \frac{l_m b^3}{8\pi^3 n^3} \right] + 1.202 \frac{l_m b^3}{8\pi^3} + \frac{b}{\pi} \left(\log \frac{b|p_m|}{4\pi} + \gamma \right) + j \frac{b}{2} \right)$$

(A19)

3. Contribution of the line located at OX-axis

The term C_3 has form of the series [5, 52]:

$$C_3 = \frac{1}{2\pi a^3} \sum_{m \neq 0} \left(\frac{1}{|m|^3} + \frac{jka}{m^2} \right) e^{-j(k|am| + q_x am)}. \quad (\text{A20})$$

These series have convergence which is not enough for effective direct numerical calculations. We will use convergence acceleration technique presented in [51] in order to evaluate these series. The dominant series can be extracted in the following way:

$$\sum_{m=1}^{+\infty} \left(\frac{1}{m^3} + \frac{jka}{m^2} \right) e^{-jkm} = \sum_{m=1}^{+\infty} \left(\frac{1}{m^3} + \frac{jka}{m^2} - \frac{jka}{m(m+1)} \right)$$

$$- \frac{jka + 1}{m(m+1)(m+2)} \Big) e^{-jkm} + jka \sum_{m=1}^{+\infty} \frac{e^{-jkm}}{m(m+1)} + (jka + 1) \sum_{m=1}^{+\infty} \frac{e^{-jkm}}{m(m+1)(m+2)} \quad (\text{A21})$$

The first series in the right-hand side of (A21) (that containing the expression in prances) can be simplified up to

$$\sum_{m=1}^{+\infty} \frac{(2jka + 3)m + 2}{m^3(m+1)(m+2)} e^{-jkm}.$$

These series have convergence $1/m^4$ which is convenient for rapid calculations. The other series in the right-hand side of (A21) can be evaluated in the closed form using the formula (A14):

$$\sum_{m=1}^{+\infty} \frac{e^{-jkm}}{m(m+1)} = \sum_{m=1}^{+\infty} \frac{e^{-jkm}}{m} - \sum_{m=1}^{+\infty} \frac{e^{-jkm}}{m+1}$$

$$= -(1 - e^{js}) \log(1 - e^{-js}) + 1,$$

$$\sum_{m=1}^{+\infty} \frac{e^{-jkm}}{m(m+1)(m+2)}$$

$$= \frac{1}{2} \left[\sum_{m=1}^{+\infty} \frac{e^{-jkm}}{m(m+1)} - \sum_{m=1}^{+\infty} \frac{e^{-jkm}}{(m+1)(m+2)} \right]$$

$$= -\frac{1}{2} \left[(1 - e^{js})^2 \log(1 - e^{-js}) + e^{js} - \frac{1}{2} \right].$$

After these manipulations the formula (A21) transforms as follows:

$$C_3 = \frac{1}{4\pi a^3} \left[4 \sum_{m=1}^{+\infty} \frac{(2jka + 3)m + 2}{m^3(m+1)(m+2)} e^{-jkam} \cos(q_x am) \right.$$

$$\left. - (jka + 1) (t_+^2 \log t^+ + t_-^2 \log t^- + 2e^{jka} \cos(q_x a)) \right. \quad (\text{A22})$$

$$\left. - 2jka (t_+ \log t^+ + t_- \log t^-) + (7jka + 3) \right],$$

where

$$t^+ = 1 - e^{-j(k+q_x)a}, \quad t^- = 1 - e^{-j(k-q_x)a},$$

$$t_+ = 1 - e^{j(k+q_x)a}, \quad t_- = 1 - e^{j(k-q_x)a}.$$

The expression (A22) looks more cumbersome as compared to the initial formula (A20), but it is much more convenient for rapid calculations. The estimations show that in order to get accuracy of 0.01% one needs to take more than 200 terms in expression (A20) and only 10 terms in (A22).

4. Energy conservation

In this subsection we evaluate the imaginary part of C and consider the problem of the energy balance in a 1D array (chain) of dipoles, in a 2D array (grid) and in a 3D array (lattice).

Let us return to formula (A20) and find the imaginary part of the interaction constant of the dipole chain:

$$\text{Im}(C_3) = \frac{2}{2\pi a^3} \sum_{m=1}^{\infty} \cos q_x a m \left(\frac{\sin kam}{m^3} - ka \frac{\cos kam}{m^2} \right). \quad (\text{A23})$$

To calculate these series we used the auxiliary formulas

$$\sum_{m=1}^{+\infty} \frac{\cos sm}{m^2} = \frac{(\pi - s')^2}{4} - \frac{\pi^2}{12}, \quad (\text{A24})$$

$$\sum_{m=1}^{+\infty} \frac{\sin sm}{m^3} = \frac{s'^3 - 3\pi s'^2 + 2\pi^2 s'}{12}. \quad (\text{A25})$$

These formulas can be easily obtained from the relation (A14) rewritten for the case $\alpha = js$

$$\begin{aligned} \sum_{m=1}^{+\infty} \frac{e^{-jsm}}{m} &= -\log(1 - e^{-js}) \\ &= -\left(\log \left| 2 \sin \frac{s}{2} \right| + j \frac{\pi - s'}{2} \right), \end{aligned} \quad (\text{A26})$$

where $s' = 2\pi\{s/(2\pi)\}$ and we use notation $\{x\}$ for fractional part of variable x . To derive (A24) and (A25) one should integrate (A26) by parameter s .

Note, that real part of C_3 contain series

$$\sum_{m=1}^{+\infty} \frac{\sin sm}{m^2}, \quad \text{and} \quad \sum_{m=1}^{+\infty} \frac{\cos sm}{m^3}, \quad (\text{A27})$$

which can be expressed in terms on second and third order repeating integrals of tangent function. These integrals can not be evaluated in elementary functions, but they are suitable for numerical calculations. We prefer to use the acceleration technique leading to the result (A22) for evaluation of C_3 , rather than to use numerical integration. Some other recommendations for calculation of series (A27) can be found in [31] together with their expansions into Taylor series.

After substitution of (A24) and (A25) into (A23) and some algebra the following compact form for $\text{Im}(C_3)$ can be obtained:

$$\text{Im}(C_3) = \frac{k^3}{6\pi} + \frac{1}{4a} \sum_{|k_x^{(m)}| < k} p_m^2. \quad (\text{A28})$$

It is easy to obtain the imaginary parts of C_2 and C_1 . The imaginary part of formula (A19) reads as:

$$\text{Im}(C_2) = \sum_{\text{Im}(k_z^{(mn)})=0} \frac{p_m^2}{2abk_z^{(mn)}} - \sum_{|k_x^{(m)}| < k} \frac{p_m^2}{4a}. \quad (\text{A29})$$

The imaginary part of formulae (A5) reads:

$$\text{Im}(C_1) = - \sum_{\text{Im}(k_z^{(mn)})=0} \frac{p_m^2}{2abk_z^{(mn)}}. \quad (\text{A30})$$

Collecting together (A28), (A29) and (A30) we obtain that

$$\text{Im}(C) = \frac{k^3}{6\pi}. \quad (\text{A31})$$

This relation makes dispersion equation (13) real valued for the case of propagating modes.

Now, let us discuss the energy balance in the chain using the result (A28). If the dipoles are arranged in a periodical linear array $x = am$ phased by wave vector with the x -component q_x (as in [52]) then the structure radiates cylindrical waves. The number of these waves depends on the relation between the wavelength, chain period and phase constant q_x . In the regime of the guided mode $q_x > k$ this number is zero since $|k_x^{(m)}| > k$ for all m . Using the Sipe-Kranendonk condition (2) for the imaginary part of the polarizability's inverse value one can obtain a purely real valued dispersion equation for the guided mode in the chain [5, 52]:

$$\mu_0 \alpha^{-1}(\omega) - C_3(\omega, q_x, a) = 0$$

However, the arrangement of the dipoles into an array changes the radiation losses of the individual scatterers. The effective polarizability of the scatterer in the linear array becomes as follows:

$$\alpha_1 = (\alpha^{-1} - \mu_0^{-1} C_3)^{-1}.$$

The Sipe-Kranendonk condition in the general case of radiated waves should be replaced by

$$\text{Im}(\alpha_1^{-1}) = \sum_{|k_x^{(m)}| < k} \frac{-p_m^2}{4a\mu_0}. \quad (\text{A32})$$

The expression (A32) follows from the formulae (2) and (A28). This relation expresses the balance between the radiation losses of the individual scatterer of the chain and the contribution of the chain unit cell into the radiated waves ($|k_x^{(m)}| < k$).

Now, consider a 2D grid of dipoles located at the nodes with coordinates $x = am$ and $y = bn$ and phased by real q_x and q_y , respectively. The effective polarizability of a scatterer in this planar grid is

$$\alpha_2 = (\alpha_1^{-1} - \mu_0^{-1} C_2)^{-1} = (\alpha^{-1} - \mu_0^{-1} (C_2 + C_3))^{-1}. \quad (\text{A33})$$

The formulae (A33) and (A29) allow to formulate an analogue of the Sipe-Kranendonk condition for the planar grid:

$$\text{Im}(\alpha_2^{-1}) = \sum_{\text{Im}(k_z^{(mn)})=0} \frac{-p_m^2}{2ab\mu_0 k_z^{(mn)}}. \quad (\text{A34})$$

The terms $-p_m^2/(4a\mu_0)$ corresponding to the cylindrical waves in (A32) are cancelled out by the respective terms from (A29) and replaced by terms $p_m^2/(2ab\mu_0k_z^{(mn)})$. The last ones correspond to the radiated plane-waves (Floquet harmonics with indexes (m, n) produced by the grid). The condition $\text{Im}(k_z^{(mn)}) = 0$ for the finite sum in (A34) is the radiation condition for these Floquet harmonics. Formula (A34) expresses the balance between the radiation losses of the dipole and the contribution of the grid unit cell into radiation.

In the surface wave regime, when $\text{Im}(k_z^{(mn)}) \neq 0$ for all m, n , using the Sipe-Kranendonk condition (2) one can obtain a real valued dispersion equation for the surface wave propagating along the grid:

$$\mu_0\alpha^{-1}(\omega) - \tilde{C}_2(\omega, q_x, q_y, a, b) = 0,$$

where

$$\tilde{C}_2(\omega, q_x, q_y, a, b) = C_2(\omega, q_x, q_y, a, b) + C_3(\omega, q_x, a).$$

Finally, let us consider a 3D lattice with nodes $x = am$, $y = bn$ and $z = cl$ phased by real q_x , q_y and q_z respectively. The effective polarizability of the scatterer in this lattice is

$$\alpha_3 = (\alpha_2^{-1} - C_1)^{-1} = (\alpha^{-1} - C)^{-1}. \quad (\text{A35})$$

From (A30), (A35) and (A34) we easily obtain

$$\text{Im}(\alpha_3^{-1}) = 0. \quad (\text{A36})$$

The terms $p_m^2/(2ab\mu_0k_z^{(mn)})$ in (A34) are cancelled by respective terms of (A30). Physically, it means that radiation losses of the scatterer in this lattice are zero. The lattice does not radiate power because it fills the whole space and the radiation losses of the single scatterer are compensated by the electromagnetic interaction in the lattice (as well as in the waveguide regimes of the chain and of the grid).

5. Final formula

Collecting together results (A5), (A19), (A20) we obtain the final expression for the dynamic interaction constant:

$$\begin{aligned} C(k, \mathbf{q}, a, b, c) = & - \sum_{n=1}^{+\infty} \sum_{\text{Re}(p_m) \neq 0} \frac{p_m^2}{\pi a} K_0(p_m b n) \cos(q_y b n) \\ & + \sum_{m=-\infty}^{+\infty} \sum_{n=-\infty}^{+\infty} \frac{p_m^2}{2jabk_z^{(mn)}} \frac{e^{-jk_z^{(mn)}c} - \cos q_z c}{\cos k_z^{(mn)}c - \cos q_z c} \quad (\text{A37}) \\ & - \sum_{\text{Re}(p_m)=0} \frac{p_m^2}{2ab} \left(\frac{1}{jk_z^{(m0)}} + \sum_{n=1}^{+\infty} \left[\frac{1}{jk_z^{(m,n)}} + \frac{1}{jk_z^{(m,-n)}} \right] \right) \end{aligned}$$

$$\begin{aligned} & - \frac{b}{\pi n} - \frac{l_m b^3}{8\pi^3 n^3} \Big] + 1.202 \frac{l_m b^3}{8\pi^3} + \frac{b}{\pi} \left(\log \frac{b|p_m|}{4\pi} + \gamma \right) + j \frac{b}{2} \Big) \\ & + \frac{1}{4\pi a^3} \left[4 \sum_{m=1}^{+\infty} \frac{(2jka+3)m+2}{m^3(m+1)(m+2)} e^{-jkam} \cos(q_x am) \right. \\ & \quad \left. - (jka+1) (t_+^2 \log t^+ + t_-^2 \log t^- + 2e^{jka} \cos(q_x a)) \right. \\ & \quad \left. - 2jka (t_+ \log t^+ + t_- \log t^-) + (7jka+3) \right], \end{aligned}$$

where we use following notations (introduced above and collected here):

$$k_x^{(m)} = q_x + \frac{2\pi m}{a}, \quad k_y^{(n)} = q_y + \frac{2\pi n}{b},$$

$$p_m = \sqrt{\left(k_x^{(m)}\right)^2 - k^2}, \quad l_m = 2q_y^2 - p_m^2,$$

$$k_z^{(mn)} = -j \sqrt{\left(k_x^{(m)}\right)^2 + \left(k_y^{(n)}\right)^2 - k^2}.$$

$$t^+ = 1 - e^{-j(k+q_x)a}, \quad t^- = 1 - e^{-j(k-q_x)a},$$

$$t_+ = 1 - e^{j(k+q_x)a}, \quad t_- = 1 - e^{j(k-q_x)a}.$$

The calculations using (A37) can be restricted to the real part only, because its imaginary part is predefined by (A31). The series in (A37) have excellent convergence that ensure very rapid numerical calculations.

6. Low frequency limit case

It is useful to consider the low frequency limit (when k , q_x , q_y and q_z are small as compared with $1/a$, $1/b$ and $1/c$) and show that the result for C transits to the known one for this case. Following to definition (A20) for term C_3 we conclude, that

$$C_3 = \frac{1}{\pi a^3} \sum_{m=1}^{+\infty} \frac{1}{m^3} = \frac{1.202}{\pi a^3}.$$

The expression (A19) for C_2 reduces to

$$C_2 = -\frac{8\pi}{a^3} \sum_{m=1}^{+\infty} \sum_{n=1}^{+\infty} m^2 K_0 \left(\frac{2\pi m}{a} b n \right).$$

Note, that both C_3 and C_2 turn out to be independent on k and \mathbf{q} . The formula (A5) for C_1 splits into the two

terms: the first one which depend on k and \mathbf{q} (where we have expanded trigonometric functions into Taylor series) and some additional constant:

$$C_1 = -\frac{1}{abc} \frac{k^2 - q_x^2}{k^2 - q_x^2 - q_y^2 - q_z^2} - \frac{4\pi}{a^2 b} \sum_{m=1}^{+\infty} \frac{m}{e^{2\pi mc/a} - 1} - \frac{8\pi}{a^3} \sum_{m=1}^{+\infty} \sum_{n=1}^{+\infty} \frac{m^2 / \sqrt{(bm/a)^2 + n^2}}{e^{2\pi \sqrt{(bm/a)^2 + n^2} c/b} - 1}$$

Finally, we get

$$C = -\frac{1}{abc} \frac{k^2 - q_x^2}{k^2 - q_x^2 - q_y^2 - q_z^2} + C_s(a, b, c), \quad (\text{A38})$$

where $C_s(a, b, c)$ is static interaction constant (7), and obtain alternative representation for $C_s(a, b, c)$:

$$C_s(a, b, c) = \frac{1.202}{\pi a^3} - \frac{8\pi}{a^3} \left[\sum_{m=1}^{+\infty} \sum_{n=1}^{+\infty} \frac{m^2 / \sqrt{(bm/a)^2 + n^2}}{e^{2\pi \sqrt{(bm/a)^2 + n^2} c/b} - 1} \right]$$

$$+ \frac{a}{2b} \sum_{m=1}^{+\infty} \frac{m}{e^{2\pi mc/a} - 1} + \sum_{m=1}^{+\infty} \sum_{n=1}^{+\infty} m^2 K_0 \left(\frac{2\pi m}{a} bn \right) \quad (\text{A39})$$

The static interaction constant expressed as (A39) is equivalent to (7). The expression (A39) can be obtained from (7) applying Poisson summation formula by index n and then by direct summation by index l (in the same manner as it was done above during evaluation of term C_1). Both formulae (A39) and (7) are extremely effective for rapid numerical calculations due to excellent convergence of the series. The difference between (7) and (A39) is that (7) contains triple series in contrast to (A39) which comprises only double ones. Noteworthy, that convergence of series in (7) is higher than in (A39).

Formula (A38) being substituted into (13) reduces the dispersion equation for an electromagnetic crystal to the known dispersion equation of a continuous uniaxial magnetic (8) with magnetic permittivity of the form (6). This fact is an important verification of introduced dispersion theory.